

DeViDe: Faceted medical knowledge for improved medical vision-language pre-training

Haozhe Luo^{1,†}, Ziyu Zhou^{2,†}, Corentin Royer¹, Anjany Sekuboyina^{1,*}, and Bjoern Menze^{1,*}

¹ Department of Quantitative Biomedicine, University of Zurich, Zurich, Switzerland

² Shanghai Jiao Tong University, Shanghai, China

Abstract. Vision-language pre-training for chest X-rays has made significant strides, primarily by utilizing paired radiographs and radiology reports. However, existing approaches often face challenges in encoding medical knowledge effectively. While radiology reports provide insights into the current disease manifestation, medical definitions (as used by contemporary methods) tend to be overly abstract, creating a gap in knowledge. To address this, we propose DeViDe, a novel transformer-based method that leverages radiographic descriptions from the open web. These descriptions outline general visual characteristics of diseases in radiographs, and when combined with abstract definitions and radiology reports, provide a holistic snapshot of knowledge. DeViDe incorporates three key features for knowledge-augmented vision language alignment: First, a large-language model-based augmentation is employed to homogenise medical knowledge from diverse sources. Second, this knowledge is aligned with image information at various levels of granularity. Third, a novel projection layer is proposed to handle the complexity of aligning each image with multiple descriptions arising in a multi-label setting. In zero-shot settings, DeViDe performs comparably to fully supervised models on external datasets and achieves state-of-the-art results on three large-scale datasets. Additionally, fine-tuning DeViDe on four downstream tasks and six segmentation tasks showcases its superior performance across data from diverse distributions.

Keywords: Vision-language Pre-training · Radiology · Medical imaging

1 Introduction

Despite the rapid evolution of deep learning models for medical diagnostics, the translation of foundational vision-language pre-training (VLP) models into practical clinical applications remains challenging. The prevailing trend in improving the reliability of VLP in the medical domain largely centres on methodological advancements. Most approaches continue to rely solely on the direct pairing of medical images with raw report data, focusing on refining the model framework to extract and learn from these image-report pairs [7, 8, 11, 27], while ignoring other sources of knowledge that offer more granularity. The persisting issue with incorporating an external knowledge base is the data quality (especially in terms

of scarcity and noise), although some works have explored techniques to denoise raw text and integrate medical knowledge from multiple sources into the pre-training [13, 38, 41, 43], they still cannot break through the limitations of coarse granularity of knowledge and reliance on a single source.

The aforementioned limitations in utilizing medical domain knowledge prompt a crucial question: How can we augment medical VLP with medical knowledge from different sources and at different levels of granularity? To answer this question, we propose the DeVide (Definitions and Visual Descriptions), which advances the field by aligning extracted disease-related entities and multi-source knowledge with corresponding visual data. By doing so, DeVide sidesteps raw reports with complex semantic information, instead extracting medical-related entities combined with enriched domain knowledge. Since traditional VLP models are primarily trained on raw radiological reports, they struggle to encapsulate the disease-specific knowledge necessary for robust diagnostics. To inject detailed disease-specific knowledge for diagnosis, we collected a new dataset that combines radiology-entity terms with their associated visual, radiographic features, providing detailed references for diagnosis.

Our contributions are multifold: (1) We construct a novel dataset of radiology-entity terms along with their associated medical definitions and radiological visual descriptors, providing a complete and direct snapshot of medical knowledge; (2) We present a novel bi-directional transformer architecture capable of processing multiple lengthy medical descriptions. It is trained with multi-granularity losses operating at varying levels of image and text detail, without requiring additional annotations.; (3) we extensively validate our approach across multiple datasets in a zero-shot setting and in fine-tuning, achieving state-of-the-art (SOTA) results compared to five baselines.

2 Related Works

2.1 Vision-Language Pre-training (VLP)

Existing VLP methods, which can be categorized into three frameworks, have mainly focused on the development of objectives and architectures to learn multi-modal representations. The first approach is to adopt dual uni-modal encoders [18, 28, 29, 34] which are composed of separate image and text encoder. CLIP [29] and ALIGN [18] pre-trained with contrastive learning have been shown to be effective for Image-Text Retrieval (ITR) without object detectors. However, they suffer from performance degradation in other downstream tasks (e.g., Visual Question Answering (VQA), Natural Language for Visual Reasoning (NLVR)). The second approach mainly utilizes a single multi-modal encoder where concatenated text and image representations are used as input. In contrast to the former approach, these works [6, 24, 25, 32] consistently show promising results on various downstream tasks. However, these methods heavily depend on the pre-trained object detectors which are computationally inefficient. Thus, recent works have tried to replace object detectors with more efficient ones. The last category offsets the shortcomings of the previous approaches by combining them,

and achieves state-of-the-art performance. ALBEF [22] combines them by adding pre-alignment before fusing. Our method is built upon this ALBEF, but deviating from the mainstream VLPs, our attention is on the **sampling strategy** for efficient pre-training.

2.2 Medical knowledge enhanced Vision-language Pre-training

Introducing medical knowledge into VLP model training has demonstrated its effectiveness. Approaches to incorporating medical knowledge into models can be categorized as either model-based or input-based. Model-based strategies aim to replicate the practices of radiological or diagnostic procedures within the model’s design [12, 23, 34, 35]. On the other hand, input-based strategies treat medical knowledge as an additional input for computational tasks or as guidance during the model’s training process [33, 37, 38, 40, 41], a technique frequently applied in report generation tasks. Although these methods advance the knowledge-integrated training in VLP, there is still a lack of effective methods for integrating fine-grained discriminative knowledge needed for the diagnostic process.

3 Method

Given a dataset with N radiograph-report pairs, $\mathcal{D} = \{(\mathbf{x}, \mathbf{t}) | \mathbf{x} \in \mathcal{X}, \mathbf{t} \in \mathcal{T}\}$, where $\mathbf{x} \in \mathbb{R}^{H \times W}$ denotes a radiograph and \mathbf{t} denotes its corresponding radiology report. As part of our knowledge aggregation (section 3.1), we assume the availability of the definitions and visual descriptions for the medical entities related to every sample in \mathcal{D} , denoted by $\mathbf{d} = \{d_1, d_2, \dots, d_k\}$, where k denotes the number of relevant entities per data sample. Our objective is to learn a vision-language model (VLM), denoted by Φ , which when applied in a zero-shot setting can predict the likelihood of a certain disease as follows:

$$\hat{\mathbf{y}} = \Phi(\mathbf{x}, \langle \mathbf{finding} \rangle),$$

where \mathbf{x} denotes a radiograph from the test set and $\hat{\mathbf{y}}$ denotes the likelihood of the presence of a finding $\langle \mathbf{finding} \rangle$. In the following sections, we present our solution to address this problem in three stages: first, describing the curation and processing of knowledge, second, the network architecture, and third, the training procedure for aligning the multiple modalities.

3.1 Knowledge Processing

Pre-processing reports. Radiology reports are extremely noisy and several works have recommended a pre-processing step before their use. For this, we employ RadGraph [17], which takes a report (\mathbf{t}) as input and recognizes all the radiological entities in it ($e_i | i \in \{1, 2, \dots, j\}$). It also classifies each of these entities into one of the four categories (s_i): anatomy (ANAT) or observation (OBS), which can in turn be: **Definitely Present**, **Definitely Absent**, or **Uncertain**. Inspired by [41], we create the final, pre-processed report \mathbf{e} as a concatenation of all the entities and their categories, i.e. $\mathbf{e} = \{e_1, s_1, [\text{SEP}], e_2, s_2, [\text{SEP}], \dots, e_j, s_j\}$. Additionally, we also collect the M most relevant entities in the training dataset into an entity set \mathcal{E} , for which the visual descriptions are collected as described below.

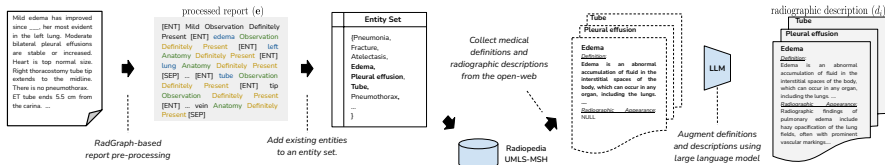


Fig. 1: Our knowledge processing pipeline involves preprocessing reports into entities and observations. Entities are queried in the Radiopaedia database for visual descriptions; if none exist, we generate a synthetic description using a Large Language Model (LLM) based on their definitions in a few-shot manner.

Collecting and processing visual descriptions. Previous works have utilized standardized medical entity descriptions (e.g. radiologist curated definitions or UMLS) as medical knowledge [31, 41]. On the other hand, trained radiologists refer to established visual descriptions of each finding in order to efficiently diagnose them. These descriptions not only contain fine-grained information about the finding but, often times, discriminative details relative to other entities. Thus, we collect detailed visual descriptions of the entities from an open-source radiology repository (Radiopaedia [1]) and use it to augment our vision-language pre-training. In order to make the collection of this knowledge tractable, we focus only on the entities in \mathcal{E} . Specifically, for every entity $e \in \mathcal{E}$, we append the MSH or NCP definition (available from UMLS) with the ‘radiographic features’ section of Radiopaedia. However, we found that the level of detail in these descriptions was not always consistent. Moreover, not all entities in \mathcal{E} contained this section. To alleviate this challenge, we augment the radiological descriptions using language-based augmentation using a large-language model. We prompt the publicly-available Mixtral-8×7B [19] with three examples of disease definitions and radiographic features (for the conditions ‘atelectasis’, ‘lung nodule’, and ‘abscess’ because the Radiopaedia data was in the desired format) and then prompt it with a new disease name to generate the relevant text. The few-shot examples help guide the format of the generated data. The prompt is presented as a conversation to the LLM:

USER: What is a [disease name]? Give me the definition.
 ASSISTANT: Definition: [disease definition]
 USER: What are the radiographic features of [disease name]?
 ASSISTANT: Radiographic features: [disease radiographic features]

This setup can be used to generate any amount of new text quickly. Using LLMs for data augmentation is a common practice that helps improve generalisability. In the medical domain, MAIRA-1 [14] uses it to generate new radiology reports, while LLaVA-Med [21] generates instruction prompts based on radiology reports. In summary, each training sample in \mathcal{D} is denoted by the triplet $\{\mathbf{x}, \mathbf{e}, \mathbf{d}\}$, where \mathbf{e} denotes the processed report and $\mathbf{d} = \{d_i\}_{i=0}^k$ denotes the set of k visual descriptions of the subset of relevant entities present in the training sample. Figure 1 gives an overview of the text-processing procedure.

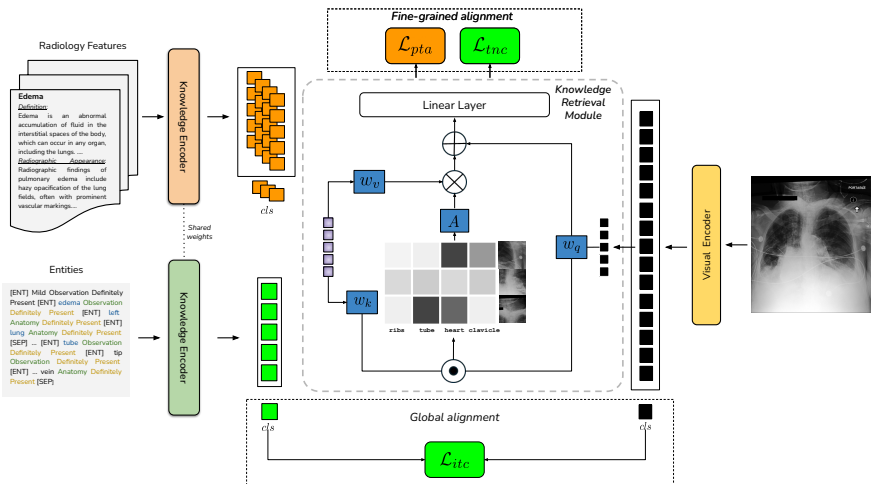


Fig. 2: The proposed DeViDe framework includes: encoding the image using a visual encoder (Sec. 3.2), entity knowledge and visual descriptors with a knowledge encoder (Sec. 3.1), capturing image-level entities-to-image correspondence using ITC loss, and employing Transformer-based Fusion layers for fine-grained alignment between image patches and visual descriptor tokens using the TNC and PTA losses (Sec. 3.3)

3.2 Network Architecture

Our model consists of two encoding streams, one for images and one shared between the pre-processed report and the radiographic descriptions. Both the image and text facets are fused into one joint feature space using a specialized cross-view fusion module and then decoded into logits resulting in likelihoods. Fig. 2 illustrates an overview of DeviDe’s architecture.

Image Encoding. We encode a radiograph using a visual backbone Φ_{image} , such as:

$$v = \Phi_{\text{image}}(\mathbf{x}) \in \mathbb{R}^{P \times d}, \quad (1)$$

where, when utilizing the vision transformer (ViT, [9]), P and d denote the number of patches into which the image is split and d denotes the feature dimension for every patch. We directly employ the last feature block of ViT-B, allowing for a richer feature representation, and leveraging the global and local contextual information. We denote ViT’s learnable `class` token by $v^{cls} \in \mathbb{R}^d$, which represents the global encoding of \mathbf{x} .

Report and Knowledge Encoding. The processed report (e) and the set of relevant radiographic descriptions (\mathbf{d}) are encoded using Med-KEBERT [41] as a pre-trained text encoder. We first tokenize e and $\{d_i\}_{i=0}^k$ and then encode them into as text embeddings. For aggregating the information from the k documents, we propose a learnable linear layer initialized with the category of the presence or absence of the entity corresponding to the description d_i . Specifically, the weight is set at 1, 0, or -1

if the entity is Definitely Present, Uncertain, or Definitely Absent. This is done so as to allow for the visual information of both the positive and negative classes to affect the training process. The report and description encoding is represented as follows:

$$t_e = \Phi_{\text{text}}(\mathbf{e}) \in \mathbb{R}^{T \times d} \quad (2)$$

$$t_d = \sum_{d_i \in \mathbf{d}} w_i \Phi_{\text{text}}(d_i) \in \mathbb{R}^{T \times d} \quad (3)$$

where T denotes the number of text tokens, d denotes the feature dimension, and w_i denotes the learnable weight of the i_{th} description embedding. Note that textual knowledge encoder also outputs the global CLS tokens, t_e^{cls} and t_d^{cls} , which contain the overall information of the reports and the descriptions.

3.3 Training

In this section, we describe the training procedure of DeViDe which aligns the image and text embeddings at varying granularity. This departs from prior works that typically align the image and text embeddings using contrastive loss.

Global radiograph-report alignment Global feature alignment between the image and the radiology report is achieved using the ubiquitous image-text contrastive loss (\mathcal{L}_{itc}), which maximizes the mutual information between the image and report representations. For this loss, we use the report embedding, which describes the overall image. Given a training radiograph-report-description triplet $(\mathbf{x}, \mathbf{e}, \mathbf{d})$, the learning objective is to maximize the similarity between the embedded image and report, specifically their CLS token. Formally,

$$\mathcal{L}_{itc} = -\log \frac{\exp(\text{sim}(v^{cls}, t_e^{cls})/\tau)}{\sum_{t_e^{cls} \in B} \exp(\text{sim}(v^{cls}, t_e^{cls})/\tau)}, \quad (4)$$

where, $\text{sim}(\cdot, \cdot)$ denotes the cosine similarity score, τ denotes the temperature scaling used for adjusting the sharpness of the distribution, and B denotes the current training batch.

Fine-grained alignment using cross-modality fusion In contrast to natural images, the information in medical images is fine-grained. More so when we are concerned about specific sub-domains, e.g. chest radiographs. In order to amplify the model’s discriminating ability on difficult cases, we choose to co-align the tokens of the radiograph with those of the report and the radiographic description using a token-level cross-attention module termed the *knowledge retrieval module* (KRM). The KRM contains multiple cross-attention layers where the key and value pairs are projections of either the report tokens or the description tokens which are queried by the visual embeddings corresponding to local patches.

Given a visual query $v \in \mathbb{R}^{P \times d}$, it is initially encoded as Q by a projection layer, while the text embedding $t \in \mathbb{R}^{T \times d}$ is encoded as K and V . Note that t could denote either t_e or t_d . The visual query Q interacts with text embeddings K and V to facilitate a fine-grained matching by computing how an image patch attends to a text token,

$$v_{pa} = \text{softmax} \left(\frac{QK^T}{\sqrt{d}} \right) V, \quad (5)$$

where $v_{pa} \in \mathbb{R}^{P \times d}$ represent the text-attended, enriched visual embeddings.

Tough negative contrastive loss is computed to enhance the model’s ability to discriminate difficult cases, inspired by metric learning. Specifically, the model is tasked to distinguish between correctly-aligned image-text pairs and closely analogous, but non-matching pairs. The learning objective for the directional alignment of image-to-text can be formalized as:

$$\mathcal{L}_{tnc}(v_{pa}, t_e) = -\log \left(\frac{\exp(s(v_{pa}, t_e))}{\exp(s(v_{pa}, t_e)) + \exp(s(v_{pa}, \bar{t}_e))} \right) \quad (6)$$

where \bar{t}_e denotes the hard-negative example within the batch B as measured by cosine similarity along the text embeddings. The scalar alignment score $s(v_{pa}, t_e)$ is computed directly from the enriched image embeddings by pooling them along the patch-dimension (P) and projecting them using a learnable, linear layer of dimension $\mathbb{R}^{1 \times d}$. Similarly, $\mathcal{L}_{tnc}(t_e, v_{pa})$ denotes the loss computed in the text-to-image direction, with negative mining in the image embedding space.

Local radiograph-description alignment is performed by tasking the model to match image patches with specific details in their radiographic description. This is done by minimizing the following cross-entropy loss aimed at patch-text alignment based on the alignment score computed as described above, albeit with a separate projection layer. Formally,

$$\mathcal{L}_{pta} = -\log \left(\frac{\exp(s(v_{pa}, t_d))}{\sum_{t'_d \in B} \exp(s(v_{pa}, t'_d))} \right) \quad (7)$$

Overall loss The overall training objective is obtained by combining the global image-text contrastive loss (Eq. 4), the fine-grained tough-negative loss (Eq. 6), and the local patch-text alignment of the radiographs and the descriptions (Eq. 7). Additionally, we support the training by employing a weakly-supervising, binary cross-entropy loss (\mathcal{L}_{bce}) if queries from \mathcal{E} appear in the report. Specifically, the names of the entities are encoded by

Phi_{text} and refined using the knowledge-retrieval module to produce the output logits. The total loss to be minimized is.

$$\mathcal{L} = \mathcal{L}_{bce} + \mathcal{L}_{itc} + \mathcal{L}_{tnc} + \alpha \mathcal{L}_{pta}, \quad (8)$$

where α regulates the contribution of radiographic descriptions to the training process.

3.4 Inference

During the inference phase, for a given test image X , the model is designed to identify specific entities or diseases. Given an entity query set q and the test image X , the process begins with encoding these inputs to generate embeddings t_q and v , respectively. Specifically, t_q is generated as the query embedding, while v is utilized as both the key and value embeddings. These embeddings are then fed into a knowledge retrieval module, which employs entity-specific visual markers to refine the query embedding, resulting in t_q^{refined} . Subsequently, an MLP layer maps the feature dimension of t_q^{refined} from d to 1, producing an output that indicates the presence or absence of each queried entity.

4 Implementation details

Pretraining. With ViT-B as the visual backbone and Med-KEBERT as the textual backbone, we pre-train on the MIMIC-CXRv2 dataset [20] on an image size of 224. We utilize the AdamW optimizer with learning rates $lr = 5 \times 10^{-5}$ and $lr_{\text{warmup}} = 1 \times 10^{-6}$. We optimize on A100 80G GPUS with a total batch size of 128 for a total of 100 epochs with the first 25 epochs for warm-up. DeViDe, pre-trained on MIMIC-CXR, is used out-of-box in a zero-shot setting for disease classification on ChestX-ray14 [36], CheXpert [15] and PadChest [5] datasets.

Finetuning. The pre-trained DeViDe can also be fine-tuned for downstream classification and segmentation tasks to evaluate its generalizability. For classification tasks, we append a randomly-initialized, linear layer to the output. Specifically, to the CLS token output for ViT-B based models and to the average-pooled feature maps from the last layer for ResNet-based models (evaluated as part of ablation). The area under the ROC curve (AUC), Matthew’s Correlation Coefficient (MCC), accuracy (ACC), and F1 metrics are used to evaluate the multi-label classification performance on NIH ChestX-ray14 [36], CheXpert [15] and Shenzhen CXR [16]). Accuracy is used to assess the multi-class classification performance (RSNA Pneumonia [2]). For the segmentation task, we use UperNet [39] as base model, replacing our pre-trained ViT-B with a randomly initialized mask prediction head and fine-tuning it on four datasets: JSRT [30], ChestX-Det [26], SIIM-ACR [3], and Montgomery [16]. In the JSRT dataset, we independently train three models, one for each of lung, heart, and clavicle. Dice is used to evaluate the segmentation performance. For fine-tuning the segmentation model, we use the AdamW optimizer with a cosine learning rate scheduler, linear warm-up of 20 epochs, and a total of 150 epochs. We employ a maximum learning rate of 0.0005 over a batch size of 64 images each of 224. We train on a single V100 16G GPU.

Baselines We evaluate our approach against a range of existing state-of-the-art (SOTA) methods for medical VLP, including ConVIRT [42], GLORIA [10], BioViL [4], CheXzero [34], Medklip [38], and KAD [41], focusing on zero-shot inference tasks. For fine-tuning, we also benchmark our model against the aforementioned methods where applicable as well as on models trained from scratch or those pre-trained on the ImageNet.

5 Results

5.1 Zero-shot setting

In this section, we evaluate our method in a zero-shot learning (ZSL) setting and compare it to relevant baselines over three prominent datasets, as recorded in Table 1. The classes evaluated in ChestXray14 and CheXpert datasets are mostly included in MIMIC-CXR and can be treated as a closed-world ZSL setup. Observe that our model outperforms all baselines methods on all metrics (except ACC). Notably, we see substantial improvement in diseases containing detailed radiographic descriptions, e.g. for Atelectasis and Edema, our model increased the AUC score by about 6%, from **0.81** to **0.87** and from **0.90** to **0.96**, respectively, surpassing CheXzero. Likewise, AUC for pleural effusion improved from **0.93** to **0.96**. When evaluating on PadChest, our model

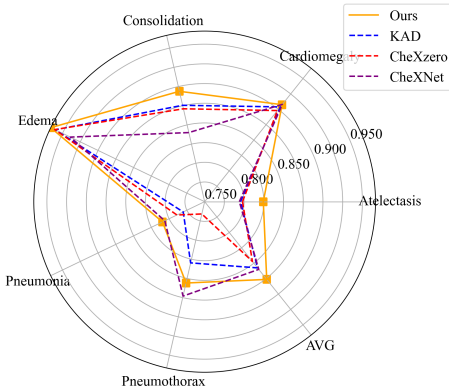


Fig. 3: The radar chart showcases our method’s AUC scores for seven PadChest diseases, demonstrating superior performance compared to previous state-of-the-art. Notably, our approach surpasses CheXNet’s fully-supervised performance despite being evaluated in a zero-shot setting.

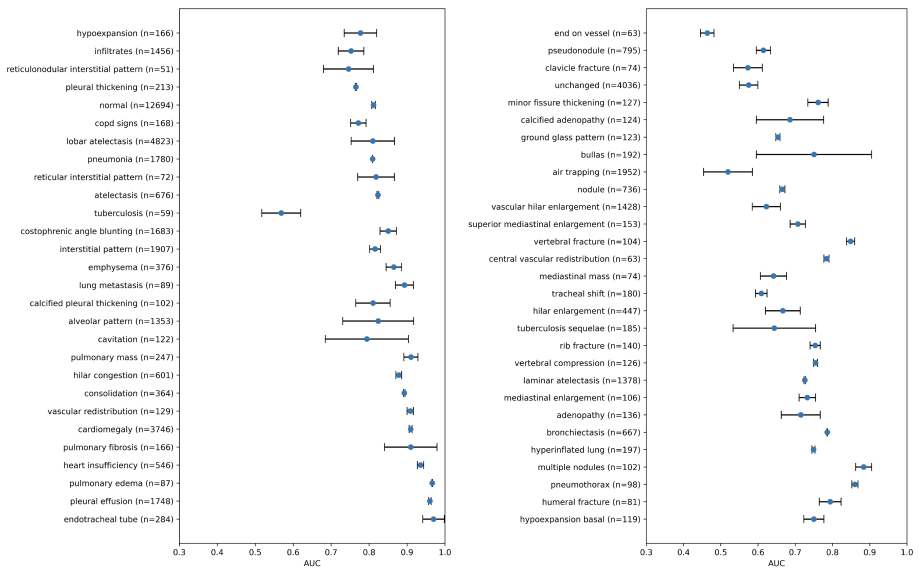


Fig. 4: In the PadChest dataset, we evaluated radiographic findings deemed high-importance by a radiologist, each with a sample size exceeding 50, presenting their mean AUC and 95% confidence intervals (CI). To ensure generalization, we externally validated our model on a subset of 39,053 human-annotated chest X-rays from PadChest, with no labeled samples from this set used during training. DeVide achieved an AUC of at least 0.900 for eight findings and at least 0.700 for 43 out of 57 findings.

achieves superior performance in **5** out of **6** unseen classes listed in CheXNet, in spite of CheXNet being fully-supervised. Our model also demonstrates better ZSL performance on other pre-trained models, as illustrated in Fig. 3. Furthermore, our model demonstrates robust performance, achieving an AUC of at least **0.90** in **eight** findings and at least **0.70** in **43** out of **56** radiographic findings within the PadChest dataset.

Table 1: Performance comparison against SOTA methods in zero-shot classification. The macro average of scores on all diseases are reported.

Methods Dataset	ChestX-ray14			Chexpert			PadChest
	AUC	F1	ACC	AUC	F1	MCC	AUC
ConVIRT	0.560	0.135	0.459	0.590	0.264	0.231	-
GLoRIA	0.610	0.174	0.503	0.750	0.570	0.501	-
BioVil	0.662	0.192	0.633	0.693	0.463	0.368	0.847
CheXzero	0.730	0.214	0.828	0.889	0.606	0.523	-
MedKlip	0.726	0.244	0.796	0.879	0.614	0.540	-
KAD	0.768	0.312	0.820	0.871	0.593	0.510	0.858
Ours	0.777	0.315	0.823	0.900	0.640	0.566	0.876

Table 2: Comparison with fully-supervised pre-trained models on different classification tasks via AUC metric.

Backbone	Pretraining data and methods	ChestX-ray14	CheXpert	ShenZhen	RSNA Pneumonia
ResNet-50	Random	80.40 \pm 0.05	86.60 \pm 0.17	90.49 \pm 1.16	70.00 \pm 0.50
	ImageNet-1K	81.70 \pm 0.15	87.17 \pm 0.22	94.96 \pm 1.19	73.04 \pm 0.35
	DeViDe	82.29 \pm 0.11	88.81 \pm 0.45	97.94 \pm 0.20	74.45 \pm 0.10
ViT-B	Random	70.84 \pm 0.19	80.78 \pm 0.13	84.46 \pm 1.65	66.59 \pm 0.39
	ImageNet-1K	77.55 \pm 1.82	83.32 \pm 0.69	91.85 \pm 3.40	71.50 \pm 0.52
	DeViDe	81.32 \pm 0.08	88.33 \pm 0.27	98.03 \pm 0.24	74.57 \pm 0.42

This showcases our model’s effectiveness in open-world disease detection in a dataset with a large domain shift. Detailed, class-wise performance is presented in Fig. 4.

The ZSL performance of DeVide highlights its robustness in handling the inherent variability in multi-center datasets, particularly with diverse range of medical entities. The high performance on open-world classes can be attributed to the transferable knowledge learnt from from radiographic descriptions during the pre-training phase.

5.2 Fine-tuning Evaluation

In this part, we start with a pre-trained model as the base and proceeding to train it comprehensively on the downstream tasks of classification and segmentation. We compare our method’s performance to that trained from scratch in a fully-supervised manner, as well as to that fine-tuned from other pre-training approaches including the standard ImageNet initialization.

Classification We conduct experiments on four distinct datasets, utilizing fractions of the data for the fine-tuning phase, in accordance with established precedents in the literature. As depicted in Table. 4, fine-tuning DeVide demonstrated significant enhancements in performance over models trained from scratch with random initialization as well as with ImageNet initialization. The performance was consistent across

Table 3: Comparison with other pre-training methods on AUC score. Different Models are end-to-end fine-tuned on the ChestX-ray14 Dataset.

Pre-training data and methods	Methods						
	ConVIRT	GLoRA	BioVil	MedKlip	KAD	PEAC	[44] DeViDe
ChestX-ray14	0.808	0.800	0.800	0.801	0.805	0.800	0.813

four distinct medical imaging datasets with both ResNet-50 and ViT-B encoders. Notably, the Vision Transformer derived greater benefits from the DeViDe pre-training, as evidenced by at least a **4%** increase in AUC scores on substantial datasets such as ChestX-ray14 and CheXpert, relative to ImageNet initialization. On the Shenzhen and RSNA Pneumonia datasets, which are smaller in scale, the benefits of our pre-training are more magnified, reaching up to a **6.2%** improvement in AUC. This shows the strong feature reuse capability of our model.

In Table. 3, we fine-tune our method as well as the other baselines on the ChestX-ray14 dataset. Our model demonstrates significantly better performance compared to the state-of-art. Despite KAD utilizing medical knowledge from UMLS and MedKLIP employing curated medical definitions, DeViDe’s superior AUC underscores the contribution of the granular, radiographic descriptions of the entities during the pre-training.

Segmentation With regards to fine-tuning a segmentation model, we widely validate the dense prediction performance on JSRT [30] for multi-organ segmentation, ChestX-Det [26] for multi-diseases conditioned segmentation, SIIM-ACR [3] for Pneumothorax segmentation and Montgomery [16] for Effusions and Miliary patterns. We transfer the pre-trained encoder, along with a randomly-initialized decoder, to each target task through end-to-end fine-tuning of all parameters. In Table. 4, we present the performance of fine-tuning based on DeViDe and compare it with that of full training from random initialization as well as ImageNet initialization. Notice that our method demonstrates a stable improvement in Dice score on different data distributions, albeit small.

Focusing on the JSRT dataset (c.f. Fig. 5a) with multi-organ segmentation, we observe a statistically significant improvement in Dice score for the lung, heart, and clavicle. It’s worth noting that DeViDe offers the highest performance gain on the clavicle, which is the most challenging class to segment among the three.

We extend the challenging clavicle segmentation task to a few-shot scenario to assess the advantages of data efficiency offered by pre-training methods. As depicted in Fig. 5b, fine-tuning based on DeViDe segmentation significantly outperforms KAD and MedKLIP by a wide margin in low-data regimes, gradually reducing the margin when all the data is utilized, while maintaining its position as the top performer.

5.3 Ablation on the losses

We conducted an ablation to study the contribution of the tough-negative sampling (\mathcal{L}_{tnc} , Eq. 6) as well as that of the radiographic (visual) descriptions of the entities (\mathcal{L}_{pta} , Eq. 7). As recorded Table. 5, we repeat the ZSL-setting on the three classification datasets without \mathcal{L}_{tnc} as well as \mathcal{L}_{pta} and observe a drop in performance. For example, the classification accuracy drops by more than 3% on two datasets without local

Table 4: Comparison with fully-supervised pre-trained model on different downstream segmentation tasks via Dice score.

Backbone	Pretraining data and methods	CheXDet	SIIM	Montgomery
ViT-B	Random	57.78 ± 0.24	72.21 ± 1.70	92.03 ± 0.20
	ImageNet-1K	69.70 ± 0.17	73.06 ± 0.76	96.59 ± 0.11
	DeViDe	70.27±0.08	75.52±0.46	96.75±0.08

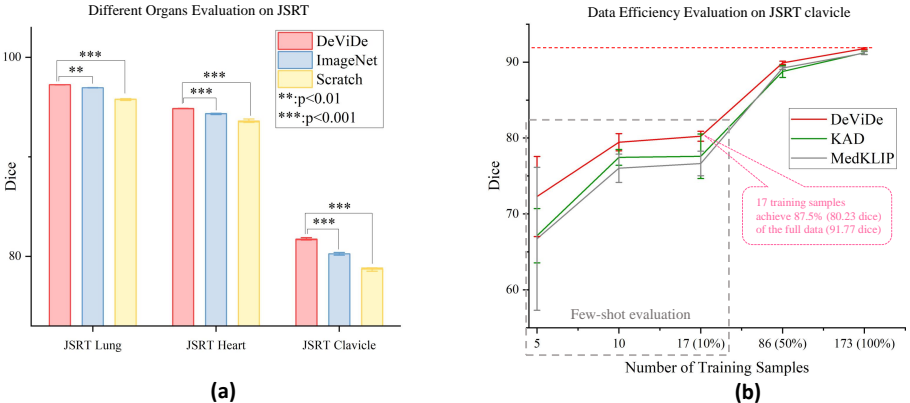


Fig. 5: Evaluation of segmentation ability across organs and few-shot segmentation under full fine-tuning setting. (a) The bar chart compares Dice coefficients of different training approaches for lung, heart, and clavicle segmentation using the JSRT dataset. Our method significantly outperforms others, with the clavicle segmentation task gaining the most. (b) The line graph assesses data efficiency in few-shot learning, focusing on the JSRT clavicle dataset. DeViDe achieves a Dice coefficient close to full dataset performance with just 17 training samples, highlighting its few-shot learning capability.

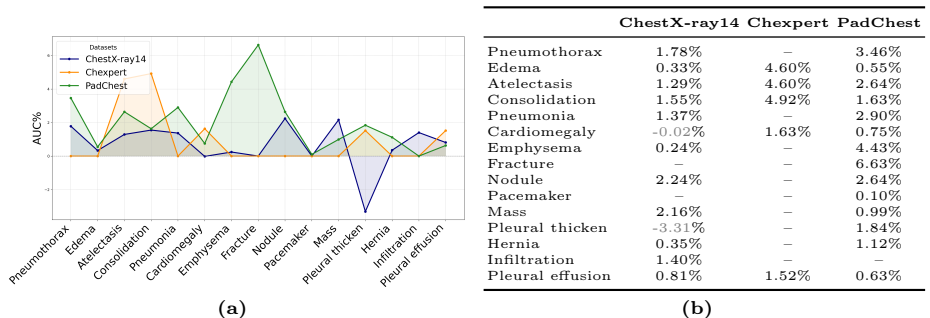
patch-text alignment. Furthermore, we explored how the injection of visual description of radiology entities enhances the zero-shot inference. In Fig. 6, we present an entity-wise ‘performance gain’ contributed by \mathcal{L}_{pta} across the entities common among the three test datasets and the relevant entity set \mathcal{E} , which are augmented by the description. Except in two instances of ChestX-ray14, we see that the image-to-description alignment consistently provides a positive performance boost, in some cases up to 6.6% in AUC (Fracture class on PadChest).

5.4 Qualitative Analysis

Visual grounding of diseases. Vision-language models offer inherent explainability in terms of visual grounding of the findings in the radiographs, thanks to the cross-attention layer. In Fig. 7, we illustrate this grounding on the test set of CheX-Det dataset, which also consists of bounding boxes for the abnormal regions. Specifically, we plot the attention mask of the knowledge retrieval layer as employed during inference with the class name as the text input. Observe the perfect localization of the

Table 5: Ablation study delineating the impact on the zero-shot learning capability of DeVide without TNC and PTA losses.

Methods	ChestXray14			CheXpert			PadChest
	AUC	MCC	ACC	AUC	MCC	ACC	AUC
DeViDe	0.7771	0.2699	0.8228	0.8998	0.5660	0.8825	0.7465
w/o \mathcal{L}_{pta}	0.7730	0.2571	0.7874	0.8965	0.5364	0.8538	0.7397
w/o \mathcal{L}_{pta} and \mathcal{L}_{tnc}	0.7689	0.2614	0.8250	0.8707	0.5163	0.8663	0.7348

**Fig. 6:** Evaluation of radiologic descriptions’ impact on zero-shot inference. (a) Plot shows AUC score enhancements for various pathologies post knowledge injection using descriptions, (b) Corresponding data table lists specific AUC improvements for pathologies within multiple datasets.

abnormalities is the diverse set of examples. Interestingly, observe the diffused nature of attention for ‘Diffuse Nodule’ and the localized attention for ‘Nodule’, which highlights the strength of granular training.

Image-to-description matching. Finally, we check how the descriptions attend to the image regions. Similar to visual grounding, we extract attention from the knowledge-retrieval layer. However, now the encoded text is the visual descriptions of the findings, as shown in Fig. 8. Notice the correspondence between the level of detail in the description to the broadness of the heatmap, for e.g. With Atelectasis, the attention to lungs is broader while that to lobes is narrower. Therefore, the description provides supplementary knowledge from which discriminative features can eventually be inferred.

6 Conclusion

In this study, we present DeVide, an novel Vision-Language Pre-training (VLP) model that enhances medical pre-training with multi-faceted knowledge: reports, medical definitions, and visual descriptions of radiology entities. We encode these facets into the model by guiding its training using tailored loss objectives aligning for global and local alignment. DeVide has undergone thorough evaluation in a zero-shot setting, where it showed a significantly superior performance relative to prior work on three datasets. When fine-tuned with DeVide’s initialization, both classification and segmentation

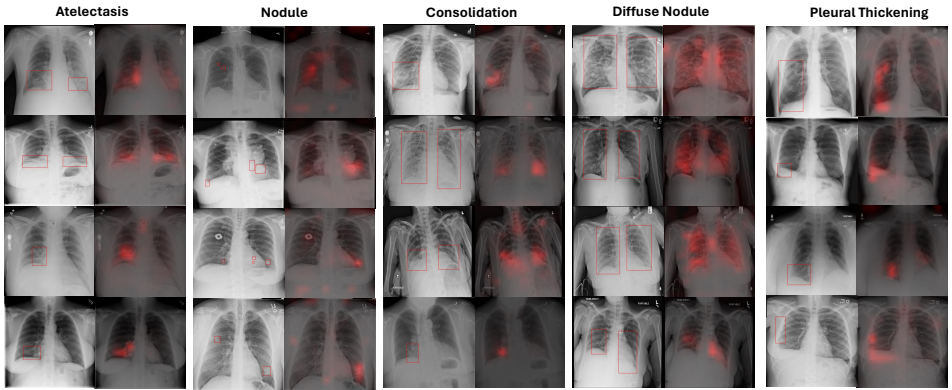


Fig. 7: Zero-shot visual grounding of diseases in findings using samples from the ChestX-Det dataset. It’s noteworthy that the attention for ‘diffuse nodule’ is dispersed, whereas the attention on ‘nodule’ is concentrated.

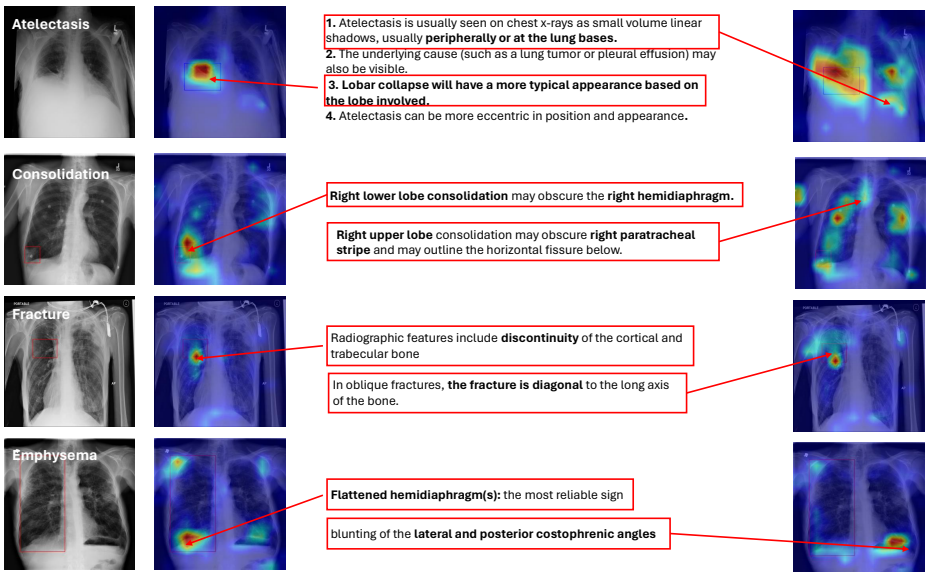


Fig. 8: Image-to-description matching by sentence-level visual attention on images randomly chosen samples from ChestX-Det dataset. Observe that the attention corresponds to the sentence while being complementary to the finding class.

tasks converged to a better optimum in terms of their performance. In a few-shot setting, DeVide-initialization was even shown to be more data efficient. Finally, through ablation studies and qualitative analysis, we indicate that the contribution of detailed radiographic visual descriptions is paramount in this performance gain.

References

1. <https://radiopaedia.org/>, the wiki-based collaborative Radiology resource. 4
2. <https://www.kaggle.com/c/rsna-pneumonia-detection-challenge>, rSNA pneumonia detection challenge (2018). 8
3. <https://www.kaggle.com/competitions/siim-acr-pneumothorax-segmentation>, sIIM-ACR Pneumothorax Segmentation (2019). 8, 11
4. Boecking, B., Usuyama, N., Bannur, S., Castro, D.C., Schwaighofer, A., Hyland, S., Wetscherek, M., Naumann, T., Nori, A., Alvarez-Valle, J., et al.: Making the most of text semantics to improve biomedical vision–language processing. In: European conference on computer vision. pp. 1–21. Springer (2022) 8
5. Bustos, A., Pertusa, A., Salinas, J.M., De La Iglesia-Vaya, M.: Padchest: A large chest x-ray image dataset with multi-label annotated reports. *Medical image analysis* **66**, 101797 (2020) 8
6. Chen, Y.C., Li, L., Yu, L., El Kholy, A., Ahmed, F., Gan, Z., Cheng, Y., Liu, J.: Uniter: Universal image-text representation learning. In: European conference on computer vision. pp. 104–120. Springer (2020) 2
7. Chen, Z., Diao, S., Wang, B., Li, G., Wan, X.: Towards unifying medical vision-and-language pre-training via soft prompts. arXiv preprint arXiv:2302.08958 (2023) 1
8. Dai, T., Zhang, R., Hong, F., Yao, J., Zhang, Y., Wang, Y.: Unichest: Conquer-and-divide pre-training for multi-source chest x-ray classification. arXiv preprint arXiv:2312.11038 (2023) 1
9. Dosovitskiy, A., Beyer, L., Kolesnikov, A., Weissenborn, D., Zhai, X., Unterthiner, T., Dehghani, M., Minderer, M., Heigold, G., Gelly, S., et al.: An image is worth 16x16 words: Transformers for image recognition at scale. arXiv preprint arXiv:2010.11929 (2020) 5
10. Huang, S.C., Shen, L., Lungren, M.P., Yeung, S.: Gloria: A multimodal global-local representation learning framework for label-efficient medical image recognition. In: Proceedings of the IEEE/CVF International Conference on Computer Vision. pp. 3942–3951 (2021) 8
11. Huang, W., Zhou, H., Li, C., Yang, H., Liu, J., Wang, S.: Enhancing representation in radiography-reports foundation model: A granular alignment algorithm using masked contrastive learning. arXiv preprint arXiv:2309.05904 (2023) 1
12. Huang, X., Fang, Y., Lu, M., Yan, F., Yang, J., Xu, Y.: Dual-ray net: automatic diagnosis of thoracic diseases using frontal and lateral chest x-rays. *Journal of Medical Imaging and Health Informatics* **10**(2), 348–355 (2020) 3
13. Huang, Z., Bianchi, F., Yuksekgonul, M., Montine, T.J., Zou, J.: A visual–language foundation model for pathology image analysis using medical twitter. *Nature medicine* **29**(9), 2307–2316 (2023) 2
14. Hyland, S.L., Bannur, S., Bouzid, K., Castro, D.C., Ranjit, M., Schwaighofer, A., Pérez-García, F., Salvatelli, V., Srivastav, S., Thieme, A., et al.: Maira-1: A specialised large multimodal model for radiology report generation. arXiv preprint arXiv:2311.13668 (2023) 4
15. Irvin, J., Rajpurkar, P., Ko, M., Yu, Y., Ciurea-Illcus, S., Chute, C., Marklund, H., Haghgoob, B., Ball, R., Shpanskaya, K., et al.: Chexpert: A large chest radiograph dataset with uncertainty labels and expert comparison. In: Proceedings of the AAAI conference on artificial intelligence. vol. 33, pp. 590–597 (2019) 8
16. Jaeger, S., Candemir, S., Antani, S., Wang, Y.X.J., Lu, P.X., Thoma, G.: Two public chest x-ray datasets for computer-aided screening of pulmonary diseases. *Quantitative imaging in medicine and surgery* **4**(6), 475 (2014) 8, 11

17. Jain, S., Agrawal, A., Saporta, A., Truong, S.Q., Duong, D.N., Bui, T., Chambon, P., Zhang, Y., Lungren, M.P., Ng, A.Y., et al.: Radgraph: Extracting clinical entities and relations from radiology reports. arXiv preprint arXiv:2106.14463 (2021) **3**
18. Jia, C., Yang, Y., Xia, Y., Chen, Y.T., Parekh, Z., Pham, H., Le, Q., Sung, Y.H., Li, Z., Duerig, T.: Scaling up visual and vision-language representation learning with noisy text supervision. In: International conference on machine learning. pp. 4904–4916. PMLR (2021) **2**
19. Jiang, A.Q., Sablayrolles, A., Roux, A., Mensch, A., Savary, B., Bamford, C., Chaplot, D.S., Casas, D.d.l., Hanna, E.B., Bressand, F., et al.: Mixtral of experts. arXiv preprint arXiv:2401.04088 (2024) **4**
20. Johnson, A.E., Pollard, T.J., Greenbaum, N.R., Lungren, M.P., Deng, C.y., Peng, Y., Lu, Z., Mark, R.G., Berkowitz, S.J., Horng, S.: Mimic-cxr-jpg, a large publicly available database of labeled chest radiographs. arXiv preprint arXiv:1901.07042 (2019) **8**
21. Li, C., Wong, C., Zhang, S., Usuyama, N., Liu, H., Yang, J., Naumann, T., Poon, H., Gao, J.: Llava-med: Training a large language-and-vision assistant for biomedicine in one day. arxiv preprint arxiv: 2306.00890 (2023) **4**
22. Li, J., Selvaraju, R., Gotmare, A., Joty, S., Xiong, C., Hoi, S.C.H.: Align before fuse: Vision and language representation learning with momentum distillation. *Advances in neural information processing systems* **34**, 9694–9705 (2021) **3**
23. Li, L., Xu, M., Wang, X., Jiang, L., Liu, H.: Attention based glaucoma detection: A large-scale database and cnn model. In: Proceedings of the IEEE/CVF conference on computer vision and pattern recognition. pp. 10571–10580 (2019) **3**
24. Li, L.H., Yatskar, M., Yin, D., Hsieh, C.J., Chang, K.W.: Visualbert: A simple and performant baseline for vision and language. arXiv preprint arXiv:1908.03557 (2019) **2**
25. Li, X., Yin, X., Li, C., Zhang, P., Hu, X., Zhang, L., Wang, L., Hu, H., Dong, L., Wei, F., et al.: Oscar: Object-semantics aligned pre-training for vision-language tasks. In: Computer Vision–ECCV 2020: 16th European Conference, Glasgow, UK, August 23–28, 2020, Proceedings, Part XXX 16. pp. 121–137. Springer (2020) **2**
26. Lian, J., Liu, J., Zhang, S., Gao, K., Liu, X., Zhang, D., Yu, Y.: A structure-aware relation network for thoracic diseases detection and segmentation. *IEEE Transactions on Medical Imaging* **40**(8), 2042–2052 (2021) **8, 11**
27. Liu, C., Cheng, S., Chen, C., Qiao, M., Zhang, W., Shah, A., Bai, W., Arcucci, R.: M-flag: Medical vision-language pre-training with frozen language models and latent space geometry optimization. In: International Conference on Medical Image Computing and Computer-Assisted Intervention. pp. 637–647. Springer (2023) **1**
28. Lu, J., Batra, D., Parikh, D., Lee, S.: Vilbert: Pretraining task-agnostic visiolinguistic representations for vision-and-language tasks. *Advances in neural information processing systems* **32** (2019) **2**
29. Radford, A., Kim, J.W., Hallacy, C., Ramesh, A., Goh, G., Agarwal, S., Sastry, G., Askell, A., Mishkin, P., Clark, J., et al.: Learning transferable visual models from natural language supervision. In: International conference on machine learning. pp. 8748–8763. PMLR (2021) **2**
30. Shiraiishi, J., Katsuragawa, S., Ikezoe, J., Matsumoto, T., Kobayashi, T., Komatsu, K.i., Matsui, M., Fujita, H., Kodera, Y., Doi, K.: Development of a digital image database for chest radiographs with and without a lung nodule: receiver operating characteristic analysis of radiologists’ detection of pulmonary nodules. *American Journal of Roentgenology* **174**(1), 71–74 (2000) **8, 11**

31. Silva-Rodriguez, J., Chakor, H., Kobbi, R., Dolz, J., Ayed, I.B.: A foundation language-image model of the retina (flair): Encoding expert knowledge in text supervision. arXiv preprint arXiv:2308.07898 (2023) **4**
32. Su, W., Zhu, X., Cao, Y., Li, B., Lu, L., Wei, F., Dai, J.: Vl-bert: Pre-training of generic visual-linguistic representations. arXiv preprint arXiv:1908.08530 (2019) **2**
33. Tan, J., Huo, Y., Liang, Z., Li, L.: Expert knowledge-infused deep learning for automatic lung nodule detection. *Journal of X-ray Science and Technology* **27**(1), 17–35 (2019) **3**
34. Tiu, E., Talius, E., Patel, P., Langlotz, C.P., Ng, A.Y., Rajpurkar, P.: Expert-level detection of pathologies from unannotated chest x-ray images via self-supervised learning. *Nature Biomedical Engineering* **6**(12), 1399–1406 (2022) **2, 3, 8**
35. Wang, K., Zhang, X., Huang, S., Chen, F., Zhang, X., Huangfu, L.: Learning to recognize thoracic disease in chest x-rays with knowledge-guided deep zoom neural networks. *IEEE Access* **8**, 159790–159805 (2020) **3**
36. Wang, X., Peng, Y., Lu, L., Lu, Z., Bagheri, M., Summers, R.M.: Chestx-ray8: Hospital-scale chest x-ray database and benchmarks on weakly-supervised classification and localization of common thorax diseases. In: *Proceedings of the IEEE conference on computer vision and pattern recognition*. pp. 2097–2106 (2017) **8**
37. Wittmann, B., Navarro, F., Shit, S., Menze, B.: Focused decoding enables 3d anatomical detection by transformers. *Machine Learning for Biomedical Imaging* **2**, 72–95 (2023). <https://doi.org/https://doi.org/10.59275/j.melba.2023-35e6>, <https://melba-journal.org/2023:003> **3**
38. Wu, C., Zhang, X., Zhang, Y., Wang, Y., Xie, W.: Medklip: Medical knowledge enhanced language-image pre-training. medRxiv pp. 2023–01 (2023) **2, 3, 8**
39. Xiao, T., Liu, Y., Zhou, B., Jiang, Y., Sun, J.: Unified perceptual parsing for scene understanding. In: *Proceedings of the European conference on computer vision (ECCV)*. pp. 418–434 (2018) **8**
40. Xie, Y., Xia, Y., Zhang, J., Song, Y., Feng, D., Fulham, M., Cai, W.: Knowledge-based collaborative deep learning for benign-malignant lung nodule classification on chest ct. *IEEE transactions on medical imaging* **38**(4), 991–1004 (2018) **3**
41. Zhang, X., Wu, C., Zhang, Y., Xie, W., Wang, Y.: Knowledge-enhanced visual-language pre-training on chest radiology images. *Nature Communications* **14**(1), 4542 (2023) **2, 3, 4, 5, 8**
42. Zhang, Y., Jiang, H., Miura, Y., Manning, C.D., Langlotz, C.P.: Contrastive learning of medical visual representations from paired images and text. In: *Machine Learning for Healthcare Conference*. pp. 2–25. PMLR (2022) **8**
43. Zhang, Y., Gao, J., Zhou, M., Wang, X., Qiao, Y., Zhang, S., Wang, D.: Text-guided foundation model adaptation for pathological image classification. In: *International Conference on Medical Image Computing and Computer-Assisted Intervention*. pp. 272–282. Springer (2023) **2**
44. Zhou, Z., Luo, H., Pang, J., Ding, X., Gotway, M., Liang, J.: Learning anatomically consistent embedding for chest radiography. arXiv preprint arXiv:2312.00335 (2023) **11**